Orthogonal L1 Fourier Transform for Digraphs

1st Vedran Mihal
Department of Computer Science
ETH Zurich
Zurich, Switzerland
vedran.mihal@inf.ethz.ch

2nd Markus Püschel
Department of Computer Science
ETH Zurich
Zurich, Switzerland
pueschel@inf.ethz.ch

***Abstract*—We introduce a novel orthogonal Fourier basis for arbitrary directed graphs, constructed via iterative maximization of the L1-norm total variation (TV) for any chosen notion of linear TV. By leveraging the theory of L1-norm principal component analysis, the basis can be computed efficiently, and it is guaranteed to exist. We show that it spans a larger range of total variations than prior constructions and demonstrate its effectiveness in signal denoising experiments.**

***Index Terms*—graph signal processing, directed graphs, Fourier analysis, L1-norm optimization**

I. Introduction

Graph signal processing (GSP) generalizes concepts from classical signal processing [1], including Fourier basis, shift, total variation and filtering. For undirected graphs, two well established models exist: one based on the Laplacian [2] and one based on the adjacency matrix [3]. In the case of directed graphs (digraphs), difficulties arise from the fact that neither the adjacency matrix nor the Laplacian has an eigenbasis; consequently, there is no unique or universally accepted model [4]. In this work we provide a GSP model for digraphs that guarantees the existence of an orthogonal Fourier basis.

Related work. Several studies proposed a GSP model for digraphs [5]–[14], resulting in several notions of graph Fourier transforms (GFTs). However, most approaches suffer from limitations: they do not apply to all digraphs [5]–[7], lack orthogonality [5]–[8], have poor scalability [9], [10], yield multiple spectra [11], [14], or rely on complex numbers [12].

The undirected GSP models can be derived from associated notions of linear total variation (TV) [15, Table I] by deriving a basis that samples the set of possible TVs. Motivated by this, [9], [10], [16] solve optimization problems to compute a Fourier basis, but use particular notions of non-linear TV.

We also adopt the view that GFT is obtained via TV optimization, but we address the aforementioned limitations.

Contribution. We propose a novel orthogonal Fourier basis, and thus Fourier transform, for digraphs, called the L_1 *digraph Fourier basis*. We obtain it by iteratively maximizing a chosen notion of linear L_1-norm TV and leveraging the theory of L_1-norm principal component analysis. In particular:

- We propose a novel orthogonal L_1 *digraph Fourier basis* that is guaranteed to exist for all digraphs and can be computed for all notions of linear TV.
- It can be computed for digraphs up to thousands of nodes.
- We prove a fundamental property of the basis: it spans the entire range of possible total variations.
- Finally, we demonstrate its effectiveness in signal denoising experiments, where it outperforms prior models.

II. Background

We recall the basic GSP concepts and provide the background on Fourier bases obtained from TV via optimization.

Basic terms. A graph on n vertices is defined as $\mathcal{G} = (\mathcal{V}, A)$, where $\mathcal{V} = (v_1, \dots, v_n)$ is the set of vertices and $A \in \mathbb{R}^{n \times n}$ is the adjacency matrix. The element $A_{ji} = 1$ if there exists an edge from v_i to v_j, and $= 0$ otherwise. If A is symmetric, $\mathcal{G}$ is undirected; otherwise it is directed. A graph signal $\mathbf{x} = (x_1, \dots, x_n)$ assigns a value x_i to node v_i. The vertex in-degree is $\deg_{\text{in}}(v_i) = \sum_{j=1}^{n} A_{ij}$, and the associated in-degree matrix is $D_{\text{in}} = \operatorname{diag}(\deg_{\text{in}}(v_1), \dots, \deg_{\text{in}}(v_n))$. Following [7] and [14], the directed Laplacian is $L = D_{\text{in}} - A$.

Total variation. The TV of $\mathbf{x}$ is defined as:

$$\mathrm{TV}(\mathbf{x}) = \|\Delta \mathbf{x}\|_p^p, \tag{1}$$

where p is typically 1 or 2, and Δ is a chosen linear difference operator on $\mathcal{G}$ (e.g., [15, Table I]). For digraphs, commonly used TVs with $p = 1$ are the adjacency-based TV [5], which was among the first definitions proposed:

$$\mathrm{TV}(\mathbf{x}) = \left\| \left(I - \frac{A}{|\lambda_{\max}|} \right) \mathbf{x} \right\|_1, \tag{2}$$

where $\lambda_{\max}$ is the eigenvalue of A with the largest magnitude, and the TV based on the directed Laplacian [7]:

$$\mathrm{TV}(\mathbf{x}) = \|L\mathbf{x}\|_1. \tag{3}$$

Various other notions of TV have been proposed in [15, Table 1], and several non-linear TV notions in [9], [10]. Note that the adjacency TV (2) is not applicable to directed acyclic graphs, since in this case $\lambda_{\max} = 0$; instead, one can use L or the Möbius TV [17].

Fourier basis via TV optimization. For undirected graphs, the Fourier basis for the standard Laplacian model can be obtained by *iterative maximization* of the corresponding TV, i.e., $\mathrm{TV}(x) = x^\top L x = \|Bx\|_2^2$, where B is the oriented incidence matrix of the undirected Laplacian L. Here, B is interpreted as a linear difference operator Δ. More generally, for any digraph and any chosen difference operator Δ in $\mathrm{TV}(\mathbf{x}) = \|\Delta \mathbf{x}\|_2^2$, an associated Fourier basis can be computed in this way, and doing so is equivalent to computing the eigenbasis of $\Delta^\top \Delta$ [18], which always exists.

In this paper we focus on solving the same maximization problem to obtain a Fourier basis, but for the L_1-norm TV instead of the L_2-norm: $\mathrm{TV}(\mathbf{x}) = \|\Delta\mathbf{x}\|_1$. The L_1-norm TV has been widely used in classical discrete-time signal processing [19] and in the foundational GSP model of [3], which further motivates our approach. We also note that solving the problem for the L_1-norm is significantly more challenging than for the L_2-norm, which admits a straightforward solution.

Note that it is generally unclear which TV is most appropriate for a given application. Thus, if a certain TV is desired, it is important to have access to a corresponding orthogonal Fourier basis. We provide it for all digraphs and all linear notions of L_1-norm TV.

III. L1 DIGRAPH FOURIER BASIS

We provide the definition of our proposed L_1 digraph Fourier basis, along with an exact algorithm for its computation and an efficient heuristic alternative.

L1 digraph Fourier basis. For a digraph $\mathcal{G}$ on n vertices, with total variation given by $\mathrm{TV}(\mathbf{x}) = \|\Delta\mathbf{x}\|_1$, where Δ is a linear difference operator, we define an orthogonal Fourier basis as the solution $(\mathbf{v}_1, \dots, \mathbf{v}_n)$ to the following iterative optimization problem for $k = n, \dots, 1$:

$$\begin{aligned} \mathbf{v}_k = \ & \arg\max\nolimits_{\mathbf{x}} \mathrm{TV}(\mathbf{x}) = \arg\max\nolimits_{\mathbf{x}} \|\Delta\mathbf{x}\|_1 \\ & \text{s.t. } \mathbf{x} \perp \{\mathbf{v}_{k+1}, \dots, \mathbf{v}_n\},\ \|\mathbf{x}\|_2 = 1, \end{aligned} \tag{4}$$

We call the resulting orthogonal basis $V = \{\mathbf{v}_1, \dots, \mathbf{v}_n\}$ the L_1 *digraph Fourier basis*. It yields the associated Fourier transform $\mathcal{F}\mathbf{x} = V^\top\mathbf{x}$, where the ith column of V is $\mathbf{v}_i$.

As we will see later, using maximization rather than minimization is crucial to ensure the fundamental property of our basis: it covers the entire TV range.

Exact algorithm. We obtain the exact solution of (4) by applying the L_1-PCA algorithm from [20] iteratively to the orthogonal complement of the previously obtained basis vectors, which ensures the orthogonality of the basis (see Fig. 1). However, it is not practical due to its exponential complexity: line 3 conducts a search in a space of 2^n possible vectors.

Efficient algorithm. We obtain an efficient approximate algorithm by replacing the expensive line 3 of the exact algorithm (Fig. 1) with the heuristic bit-flipping (BF) procedure [21]. It replaces the exhaustive search with a converging sequence of bit-flips to find approximation of $\mathbf{b}_k$. Concretely, it replaces line 3 in Fig. 1 with lines 3a and 3b in Fig. 2.

Guarantees for the bit-flipping method are provided theoretically and experimentally in [21], including convergence proofs, time complexity, specific performance bounds (see Proposition 5), and comparisons with other state-of-the-art algorithms. The time complexity of the bit-flipping step is $\mathcal{O}(n^3)$, so the overall algorithm is in $\mathcal{O}(n^4)$. In our experiments, we were able to compute the basis for graphs with up to a few thousand vertices in reasonable time. We note that, due to the approximate nature of the algorithm, the resulting basis may need to be reordered with respect to the TV.

Input: $\Delta \in \mathbb{R}^{m\times n}$ linear graph difference operator
Output: $\mathbf{v}_1, \dots, \mathbf{v}_n$ orthogonal Fourier basis

1: $Y^{(n)} \leftarrow I_n \in \mathbb{R}^{n\times n}$
2: **for** $k \leftarrow n$ **downto** 2 **do**
3: $\quad \mathbf{b}_k = \arg\max_{\mathbf{b}\in\{\pm 1\}^n} \left\|(\Delta Y^{(k)})^\top \mathbf{b}\right\|_2$
4: $\quad \mathbf{v}_k = Y^{(k)} \cdot \frac{(\Delta Y^{(k)})^\top \mathbf{b}_k}{\left\|(\Delta Y^{(k)})^\top \mathbf{b}_k\right\|_2}$
5: $\quad Y^{(k-1)} \leftarrow [\mathbf{y}_1^{(k-1)}, \dots, \mathbf{y}_{k-1}^{(k-1)}] \in \mathbb{R}^{n\times(k-1)}$ orthogonal basis of $\mathrm{span}\,(\mathbf{v}_k, \dots, \mathbf{v}_n)^\perp$
6: **end for**
7: $\mathbf{v}_1 \leftarrow \mathbf{y}_1^{(1)}$

Fig. 1: The exact L_1 digraph Fourier basis algorithm.

3a: $(U, \Sigma, V) \leftarrow \mathrm{compactSVD}(\Delta Y^{(k)}),\ Z \leftarrow \Sigma U^\top$ [22]
3b: $\mathbf{b}_k = \mathrm{BF}\left(Z^\top Z,\ \mathrm{sgn}([Z]_{:,1})\right)$ [21]

Fig. 2: The efficient L_1 digraph Fourier basis algorithm replaces line 3 in Fig. 1 by lines 3a and 3b. The latter uses the bit-flipping method (BF) [21] to efficiently find an approximation of $\mathbf{b}_k$. See [21] for details.

Example. Fig. 3 shows the first three (low frequency) vectors of the exact and the efficient L_1 digraph Fourier basis according to the adjacency TV (2), for a 20-vertex digraph. The efficient basis vectors are close to the exact ones.

IV. COVERING THE TV RANGE

For a given TV, it is crucial that the Fourier basis samples the entire range of TVs, and the low (TV) frequencies in particular, since it affects the associated spectral analysis, use of filters, and any Fourier based method [9]. To this end, we prove the key theoretical guarantee of our L_1 Fourier basis: it spans the *entire range of TV values*. Specifically, this means that the L_1 Fourier basis contains vectors achieving both the minimum and the maximum possible TV. We note that this is generally not the case when using TV minimization rather than maximization.

By construction, the first computed basis vector $\mathbf{v}_n$ always attains the maximum TV, and the efficient algorithm provides a good approximation (see [21]). Surprisingly, the last computed vector $\mathbf{v}_1$ for *both* the exact and the efficient algorithm always has $\mathrm{TV}(\mathbf{v}_1) = 0$, provided this is permitted by the operator Δ, i.e., $\mathrm{rank}(\Delta) < n$[1], which is commonly the case (e.g., in (2)[2] and (3)). Importantly, this holds for both the exact and the efficient algorithm.

Theorem 1. *The L_1 Fourier basis vector $\mathbf{v}_1$ attains the minimum possible TV of zero when $\mathrm{rank}(\Delta) < n$, for both the exact and the efficient algorithm.*

Proof. We use notation from Fig. 1, so $Y^{(k)} = [\mathbf{y}_1^{(k)}, \dots, \mathbf{y}_k^{(k)}]$ is an orthogonal basis of $\mathrm{span}(\mathbf{v}_{k+1}, \dots, \mathbf{v}_n)^\perp$. We show

[1] If $\mathrm{rank}(\Delta) = n$, the only signal with zero total variation is the all-zero signal. This case does not occur with most common notions of total variation.

[2] For unweighted or nonnegatively weighted digraphs, the Perron-Frobenius theorem [23] implies $\mathrm{rank}\left(I - \frac{A}{|\lambda_{\max}|}\right) < n$.

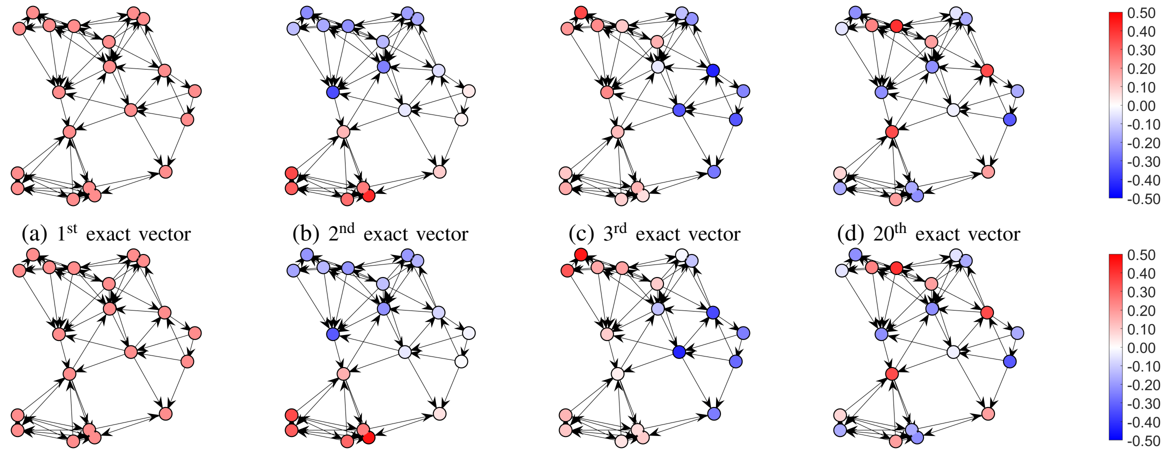

(a) 1st exact vector (b) 2nd exact vector (c) 3rd exact vector (d) 20th exact vector

(e) 1st efficient vector (f) 2nd efficient vector (g) 3rd efficient vector (h) 20th efficient vector

Fig. 3: The first three and the last basis vector of the exact and the efficient L_1 digraph Fourier basis on a 20-vertex digraph.

inductively for $k \in \{n, n-1, \ldots, 2\}$, that after the $(n-k+1)$th iteration of the for-loop, $\operatorname{span}(\mathbf{y}_1^{(k-1)}, \ldots, \mathbf{y}_{k-1}^{(k-1)})$ contains a non-zero vector with zero TV. Thus, $\mathbf{v}_1 = \mathbf{y}_1^{(1)}$ has zero TV.

For $k = n$, the space spanned by $\mathbf{y}_1^{(n)}, \ldots, \mathbf{y}_k^{(n)}$ is $\mathbb{R}^n$, so it contains a non-zero vector with zero TV (as $\operatorname{rank}(\Delta) < n$). Let $\mathbf{x} \in \operatorname{span}(\mathbf{y}_1^{(k)}, \ldots, \mathbf{y}_k^{(k)})$ be a non-zero vector with zero TV (hypothesis), so $\mathbf{x} \perp \{\mathbf{v}_{k+1}, \ldots, \mathbf{v}_n\}$ and $\Delta\mathbf{x} = \mathbf{0}$. We show $\mathbf{x} \perp \mathbf{v}_k$, which implies $\mathbf{x} \in \operatorname{span}(\mathbf{y}_1^{(k-1)}, \ldots, \mathbf{y}_{k-1}^{(k-1)})$:

$$\begin{aligned}\mathbf{x}^\top \mathbf{v}_k &= \mathbf{x}^\top Y^{(k)} (Y^{(k)})^\top \Delta^\top \cdot \frac{\mathbf{b}_k}{\left\|(\Delta Y^{(k)})^\top \mathbf{b}_k\right\|_2} \\ &= (\Delta \mathbf{x})^\top \cdot \frac{\mathbf{b}_k}{\left\|(\Delta Y^{(k)})^\top \mathbf{b}_k\right\|_2} = 0.\end{aligned}$$

$Y^{(k)}(Y^{(k)})^\top \mathbf{x} = \mathbf{x}$ follows from $\mathbf{x} \in \operatorname{span}(\mathbf{y}_1^{(k)}, \ldots, \mathbf{y}_k^{(k)})$. $\square$

Combined with the fact that the L_1 Fourier basis always contains a vector with the maximum possible TV, Theorem 1 leads to the following corollary, which is the key property of the L_1 Fourier basis:

Corollary 1. *The L_1 Fourier basis covers the entire TV range for TVs associated with a rank-deficient linear operator Δ. In particular, it contains vectors achieving both the minimum and the maximum possible TV.*

Example. We illustrate the result from Corollary 1 for the adjacency TV (2) on two synthetic digraphs with 100 vertices and average in- and out-degree of 4, according to the Erdős–Rényi and Barabási–Albert models [24]. Figs. 4a and 4b show the TV range obtained with our construction (in red), compared to the range covered by the prior Fourier bases from [8]–[13]. Naturally, these are associated with different TVs and thus cover the TV range less effectively. Nevertheless, if the TV in (2) is the one of interest, our basis should be the superior choice.

V. Experiments

We evaluate the L_1 digraph Fourier basis on real-world data from the River Thames network. In particular, we perform a signal denoising experiment, followed by spectral analysis.

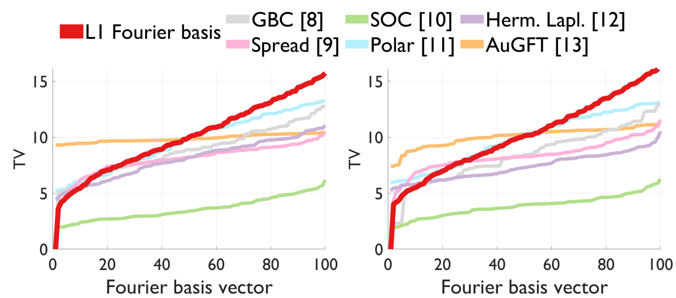

(a) TV range for Fourier bases on an Erdős–Rényi digraph. (b) TV range for Fourier bases on a Barabási–Albert digraph.

Fig. 4: TV range for various Fourier bases on an Erdős–Rényi and a Barabási–Albert digraph on 100 vertices.

Dataset. We consider the River Thames network dataset [25], which contains measurements collected weekly at multiple sites across the river network. Vertices are defined as pairs *(site, time point)*, and there are two types of directed edges: each site is connected to itself at the subsequent time point, and neighboring sites are connected at the same time point following the water flow direction. We consider two types of data: water temperature (in °C) and dissolved sulfate concentration (in $\mathrm{mg\,L^{-1}}$). Each signal consists of weekly measurements at the sites over the course of one year, i.e., there is a value associated with each vertex *(site, time point)*.

A. Signal denoising

Experimental setup. We corrupt the original signal $\mathbf{x}$ by zero-mean uncorrelated Gaussian noise $\mathbf{e}$, resulting in the noisy signal $\mathbf{y} = \mathbf{x} + \mathbf{e}$. Denoising is carried out via low-pass filtering in the frequency domain, since the signals are assumed to be low-frequency:

$$\hat{\mathbf{x}} = \mathcal{F}^{-1} \operatorname{diag}(\mathbf{h}) \mathcal{F} \mathbf{y},$$

where $\hat{\mathbf{x}}$ denotes the denoised signal, $\mathcal{F}$ is our Fourier transform obtained from the Laplacian TV (3), and $\mathbf{h} =$

$(h_1, \dots, h_n)$ is the frequency response of the filter. In particular, we consider two different filter designs, $\mathbf{h}^{(\sigma)}$ and $\mathbf{g}^{(\gamma)}$, formulated similarly to a heat kernel and the Tikhonov filter, respectively [2]:

$$(\mathbf{h}^{(\sigma)})_i = e^{-\frac{i-1}{\sigma^2}}, \quad (\mathbf{g}^{(\gamma)})_i = \frac{1}{1+\gamma\cdot(i-1)}.$$

Parameters σ and γ control the extent of the low-pass effect. Filtering is performed on a mean-centered version of the noisy signal, i.e., the mean of $\mathbf{y}$ is subtracted before denoising and reintroduced afterwards. The choice of filtering for denoising provides a broad class of denoisers, while also allowing for direct comparison between different Fourier bases.

Experiment. We denoise Thames signals, considering four signals (years 2013–2016) of each type (temperature and sulfate concentration). We report the average signal-to-noise ratio (SNR) [26] after denoising. The SNR of the noisy input $\mathbf{y}$ is set to $7\,\mathrm{dB}$; other values yielded similar results.

We compare against prior digraph Fourier transforms [7]–[13], whenever they exist and can be computed in reasonable time. We also include the Fourier transform from [27], which is applicable here since the Thames network is acyclic.

Results. Fig. 5 reports the denoising results with filters $\mathbf{h}^{(\sigma)}$ and $\mathbf{g}^{(\gamma)}$, respectively. The legend is in Fig. 5a. Each line corresponds to a different Fourier basis, with our L_1 Fourier basis shown in red. The y-axes report the average SNR after denoising, and the x-axes correspond to the filter parameters σ and γ, which we present over a relevant range where performance peaks, with different methods approaching similar values outside this region. Fourier bases that fail to improve the SNR over the noisy baseline are omitted from the plots. For the methods included, filtered signals did not perform worse than the noisy baseline for any parameter choice. In terms of computational efficiency, our method computed the basis within a few minutes, whereas, for instance, the methods from [9], [10] failed to converge within several hours. Our L_1 Fourier basis outperforms all prior bases, which demonstrates its potential for applications.

B. Spectral analysis

To gain further insight into the previous experiment, we present the spectra of two signals. Figs. 6 and 7 show the magnitude spectra of the 2016 temperature and sulfate concentration signals, respectively, normalized to a 2-norm of 1. The spectra are computed using the L_1 Fourier basis as well as other prior bases from Fig. 5. Frequency components are on the x-axis, and the y-axis shows each component's magnitude.

The spectra of both signals in the L_1 Fourier basis are strongly concentrated in the low-frequency range, which explains good denoising performance. Comparing spectra across other Fourier bases further illustrates the denoising effectiveness: bases that concentrate the spectra more strongly in the low-frequency range tend to achieve better denoising results.

(a) Legend for the denoising experiment.

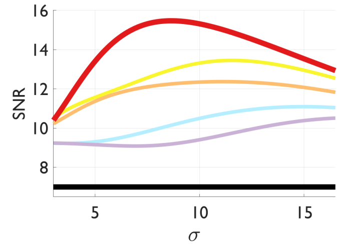

(b) Average SNR of four denoised temperature signals denoised with filter $\mathbf{h}^{(\sigma)}$.

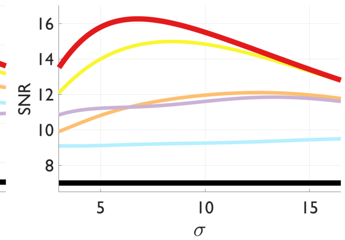

(c) Average SNR of four denoised sulfate signals denoised with filter $\mathbf{h}^{(\sigma)}$.

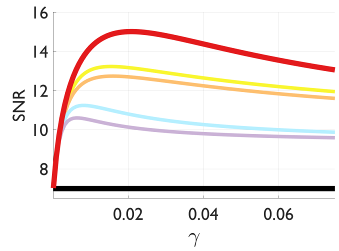

(d) Average SNR of four denoised temperature signals denoised with filter $\mathbf{g}^{(\gamma)}$.

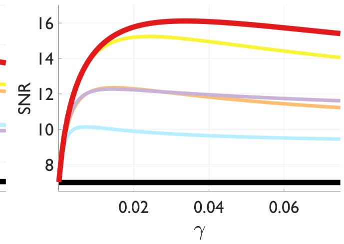

(e) Average SNR of four denoised sulfate signals denoised with filter $\mathbf{g}^{(\gamma)}$.

Fig. 5: Average SNR of Thames signals denoised with filters $\mathbf{h}^{(\sigma)}$ and $\mathbf{g}^{(\gamma)}$ across various Fourier bases.

VI. Conclusion

Digraph signal processing is not yet consolidated, since neither adjacency nor Laplacian matrix has an eigenbasis in general, preventing an obvious definition of a Fourier basis. Prior approaches to obtain a Fourier basis face issues such as non-orthogonality or limited scalability in its computation. Our proposed L_1 Fourier basis overcomes these issues: it always exists, is orthogonal, scales to graphs with thousands of nodes, and works with any L_1-norm TV operator. The basis has an appealing theoretical and practical property: it spans the full range of TVs and thus frequencies. Denoising experiments confirm its potential and motivate further research.

References

[1] A. Ortega, P. Frossard, J. Kovačević, J. M. F. Moura, and P. Vandergheynst, "Graph signal processing: Overview, challenges, and applications," *Proc. IEEE*, vol. 106, no. 5, pp. 808–828, 2018.

[2] D. I. Shuman, S. K. Narang, P. Frossard, A. Ortega, and P. Vandergheynst, "The emerging field of signal processing on graphs: Extending high-dimensional data analysis to networks and other irregular domains," *IEEE Signal Process. Mag.*, vol. 30, no. 3, pp. 83–98, 2013.

[3] A. Sandryhaila and J. M. F. Moura, "Discrete signal processing on graphs," *IEEE Trans. Signal Process.*, vol. 61, 10 2012.

[4] A. G. Marques, S. Segarra, and G. Mateos, "Signal processing on directed graphs: The role of edge directionality when processing and learning from network data," *IEEE Signal Process. Mag.*, vol. 37, no. 6, pp. 99–116, 2020.

[5] A. Sandryhaila and J. M. F. Moura, "Discrete signal processing on graphs: Frequency analysis," *IEEE Trans. Signal Process.*, vol. 62, no. 12, pp. 3042–3054, 2014.

[6] J. Domingos and J. M. F. Moura, "Graph Fourier transform: A stable approximation," *IEEE Trans. Signal Process.*, vol. 68, pp. 4422–4437, 2020.

[7] R. Singh, A. Chakraborty, and B. S. Manoj, "Graph Fourier transform based on directed Laplacian," in *Int. Conf. Signal Process. Commun.*, 2016, pp. 1–5.

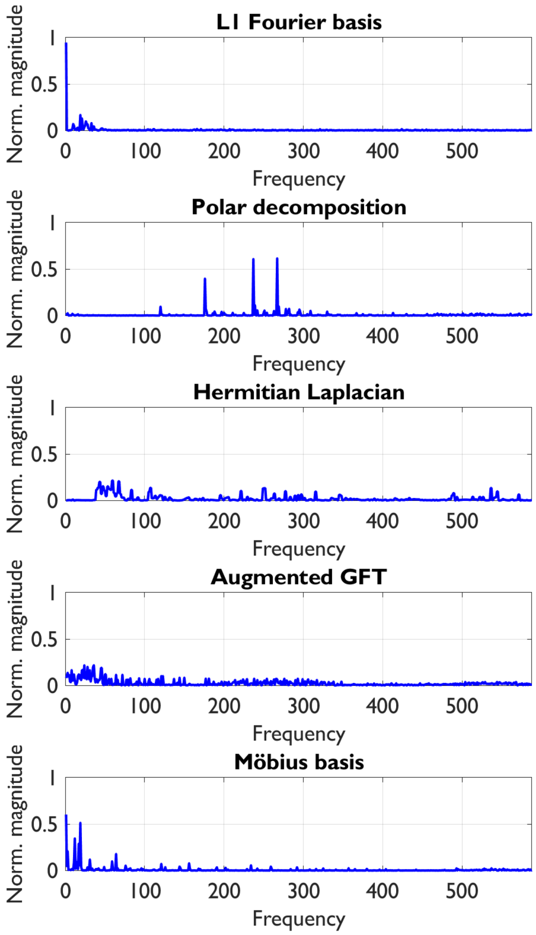

Fig. 6: Spectra of the 2016 temperature signal from the Thames network according to different Fourier bases.

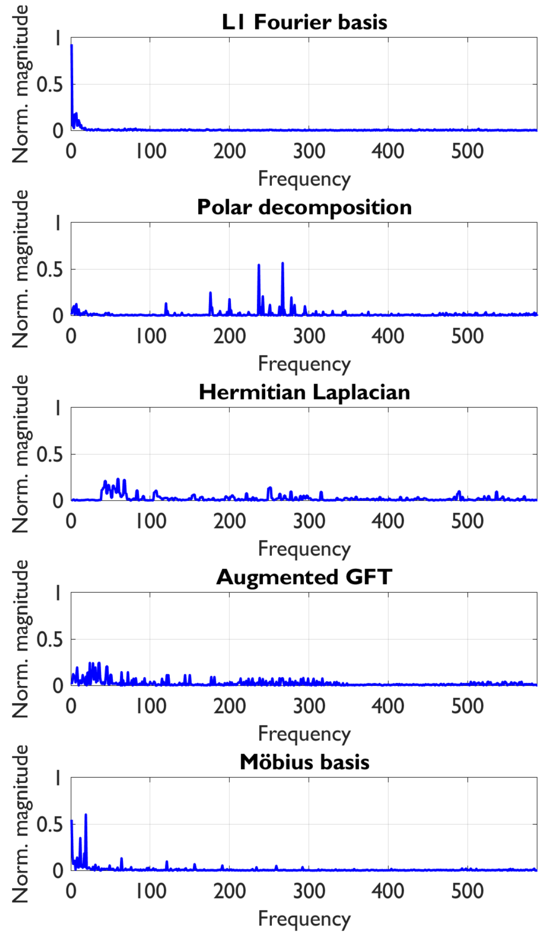

Fig. 7: Spectra of the 2016 sulfate concentration signal from the Thames network according to different Fourier bases.

[8] B. Seifert and M. Püschel, "Digraph signal processing with generalized boundary conditions," *IEEE Trans. Signal Process.*, vol. 69, pp. 1422–1437, 2021.

[9] R. Shafipour, A. Khodabakhsh, G. Mateos, and E. Nikolova, "A directed graph Fourier transform with spread frequency components," *IEEE Trans. Signal Process.*, vol. 67, no. 4, pp. 946–960, 2019.

[10] S. Sardellitti, S. Barbarossa, and P. D. Lorenzo, "On the graph Fourier transform for directed graphs," *IEEE J. Sel. Topics Signal Process.*, vol. 11, no. 6, pp. 796–811, 2017.

[11] S. Kwak, L. Shimabukuro, and A. Ortega, "Frequency analysis and filter design for directed graphs with polar decomposition," in *IEEE Int. Conf. Acoust., Speech, Signal Process.* IEEE, 2024, pp. 9661–9665.

[12] S. Furutani, T. Shibahara, M. Akiyama, K. Hato, and M. Aida, "Graph signal processing for directed graphs based on the Hermitian Laplacian," in *Proc. Europ. Conf. on Machine Learning and Principles and Practice of Knowledge Discovery in Databases (ECML PKDD)*, 2019, pp. 447–463.

[13] H. Kitamura, H. Yasuda, Y. Tanaka, and S. Muramatsu, "Realization of digraph filters via augmented GFT," in *2023 IEEE Int. Conf. Image Process. (ICIP)*. IEEE, 2023, pp. 2885–2889.

[14] Y. Chen, C. Cheng, and Q. Sun, "Graph Fourier transform based on singular value decomposition of the directed Laplacian," *Sampling Theory, Signal Process., and Data Analysis*, vol. 21, no. 2, p. 24, 2023.

[15] A. Anis, A. Gadde, and A. Ortega, "Efficient sampling set selection for bandlimited graph signals using graph spectral proxies," *IEEE Trans. Signal Process.*, vol. 64, no. 14, pp. 3775–3789, 2016.

[16] L. Yang, A. Qi, C. Huang, and J. Huang, "Graph Fourier transform based on ℓ_1 norm variation minimization," *Appl. Comput. Harmon. Anal.*, vol. 52, pp. 348–365, 2021.

[17] V. Mihal and M. Püschel, "Möbius total variation for directed acyclic graphs," in *IEEE Int. Conf. Acoust., Speech, Signal Process.* IEEE, 2023, pp. 1–5.

[18] D. Spielman, "Spectral and algebraic graph theory," *Yale lecture notes, draft of December*, vol. 4, p. 47, 2019.

[19] S. Mallat, *A wavelet tour of signal processing*. Elsevier, 1999.

[20] P. P. Markopoulos, G. N. Karystinos, and D. A. Pados, "Optimal algorithms for L1-subspace signal processing," *IEEE Trans. Signal Process.*, vol. 62, no. 19, pp. 5046–5058, 2014.

[21] P. P. Markopoulos, S. Kundu, S. Chamadia, and D. A. Pados, "Efficient L1-norm principal-component analysis via bit flipping," *IEEE Trans. Signal Process.*, vol. 65, no. 16, pp. 4252–4264, 2017.

[22] G. H. Golub and C. F. Van Loan, *Matrix computations*. JHU press, 2013.

[23] C. D. Meyer, *Matrix analysis and applied linear algebra*. SIAM, 2023.

[24] B. J. Prettejohn, M. J. Berryman, and M. D. McDonnell, "Methods for generating complex networks with selected structural properties for simulations: a review and tutorial for neuroscientists," *Front. comput. neurosci.*, vol. 5, p. 11, 2011.

[25] M. J. Bowes, L. K. Armstrong, S. A. Harman, D. J. E. Nicholls, H. D. Wickham, P. M. Scarlett, and M. D. Juergens, "Weekly water quality data from the River Thames and its major tributaries (2009-2017)," 2020, https://doi.org/10.5285/cf10ea9a-a249-4074-ac0c-e0c3079e5e45, (accessed Nov. 6, 2024). [Online]. Available: https://doi.org/10.5285/cf10ea9a-a249-4074-ac0c-e0c3079e5e45

[26] J. G. Proakis and D. G. Manolakis, *Digital signal processing (3rd ed.): principles, algorithms, and applications*. USA: Prentice-Hall, Inc., 1996.

[27] V. Mihal and M. Püschel, "Orthogonal Fourier analysis on directed acyclic graphs via Möbius total variation," *IEEE Trans. Signal Process.*, 2025.